AERODYNAMIC STIFFNESS OF AN UNBOUND ECCENTRIC WHIRLING CENTRIFUGAL IMPELLER WITH AN INFINITE NUMBER OF BLADES

Paul E. Allaire
Department of Mechanical and Aerospace Engineering
University of Virginia
Charlottesville, Virginia 22901

Lyle A. Branagan
Pacific Gas and Electric
San Ramon, California 94583

John A. Kocur
Department of Mechanical and Aerospace Engineering
University of Virginia
Charlottesville, Virginia 22901

ABSTRACT

This paper considers an unbounded eccentric centrifugal impeller with an infinite number of log spiral blades undergoing synchronous whirling in an incompressible fluid. The forces acting on it due to coriolis forces, centripetal forces, changes in linear momentum, changes in pressure due to rotating and changes in pressure due to changes in linear momentum are evaluated.

NOMENCLATURE

Symbol	Definition
$\vec{a}$	Vector acceleration
a	Impeller perturbation
b	Thickness of two-dimensional impeller
$\vec{F}_p$	Vector pressure forces
$\vec{F}_s$	Vector surface forces on control volume
$\vec{F}_{SHAFT}$	Vector force of the shaft on the fluid
ΔF_{ij}	Change in force in i direction due to perturbation in j direction
K_{xx}	Principal stiffness
$\bar{K}_{xx}$	Dimensionless principal stiffness, $(K/\rho U_{R_1} R_1)$
K_{yx}	Cross-coupled stiffness
$\bar{K}_{yx}$	Dimensionless cross-coupled stiffness
n	Number of blades

This work was supported in part by NASA Lewis Research Center, Contract No. NAG 3-180 and in part by the University of Virginia Rotating Machinery and Controls Industrial Research Program.

O	Center of flow field
O'	Geometric center of impeller
$\bar{R}$	Dimensionless radii ratio, (R_2/R_1)
R_1	Inner radius of impeller
R_2	Outer radius of impeller
R_B	Radius of impeller with respect to center of flow field
U_{R1}	Average radial inlet velocity in fixed coordinate frame
U_B	Radial velocity at point B
V_B	Relative velocity of rotating coordinate system at point B
$\vec{V}$	Analytic velocity expression for force equation
W_B	Velocity in rotating coordinate system at point B
$\vec{W}_{TOT}$	Vector velocity at any point in rotating coordinate system
β	Blade angle $(\tan\beta = U_{R_1}/\omega R_1)$
ε	Dimensionless eccentricity
θ	Angle measured from x axis
θ_1	Entrance angle
θ_2	Exit angle
θ_b	Blade sweep angle $(\theta_b = \cot\beta \ln(R_2/R_1))$
θ'	Angle of fluid particle along blade
ρ	Fluid density
ω	Angular speed of the impeller

1. INTRODUCTION

The analysis of turbomachinery requires a combination of solid mechanics and fluid dynamics. Vibrations of a centrifugal pump or compressor are controlled by the bearings, by the shaft geometry, by fluid forces on the impeller, by seals, and other factors. Often the nature and magnitude of the forces and stiffnesses generated by bearings and shaft geometry are fairly well understood and can, in general, be accurately modeled. Those forces acting on the impeller can rarely be adequately determined as yet. These forces arise from the interaction of the impeller with the driven fluid, and are often called "aerodynamic forces," "aerodynamic stiffnesses" or "aerodynamic cross-coupling".

Much of the large body of work on incompressible flows in impellers assumes a centered impeller with varying degrees of complexity. A few examples include one-dimensional velocity vectors [1], two-dimensional considerations [2,3], and full three-dimensional analysis [4,5,6]. These are not discussed further.

Calculation of aerodynamic forces was first reported by Alford [7], considering circumferential variations of static pressure and efficiency in axial compressors.

Work by Black [8], Barrett and Gunter [9], Lund [10], and Gunter, et al. [11], have demonstrated the importance of aerodynamic forces to the safe operation of turbomachinery, but have not, in general, addressed the calculation of these forces, or their associated stiffnesses. Further, in the work by Barrett [9] and Gunter [11], these forces are modeled by their cross-coupled stiffness only; consideration is not given to the principal stiffness of the fluid-impeller interaction.

Several recent papers have sought to more accurately quantify these forces. Colding-Jorgensen [12] used a simple source and vortex flow model for the impeller along with a series of vortex sheets representing the pump volute. He then superimposed a uniform flow over this model, without clear physical explanation, to determine the forces on the volute, as a function of the volute spiral angle. The flow field emerging from the impeller is assumed to correspond with the typical one-dimensional analysis, except that its location is perturbed. The force calculated by this method is the total force acting on the entire impeller/volute model for uniform flow - not the force on the impeller.

The work by Shoji and Ohashi [13] considers an ideal impeller whirling about its geometric center. Blades are modeled by vortex sheets using unsteady potential theory with shockless entry to predict the flow field within the impeller. Forces on the blades are summed from the pressures calculated by an unsteady Bernoulli equation. The calculation is two-dimensional without volute or vaned diffuser effects but does allow for a whirl frequency other than the rotational speed.

The papers by Thompsen [14,15] outline the assumptions and general theory contained in a proprietary program. The technique uses unsteady flow theory and determines the stability of the rotor stage based on nonsynchronous fluid excitations. The proprietary nature of the program limits the discussion of the details of the procedure. An actuator disc method for calculating forces is currently being used by Chamieh et al. [16]; however, the work is incomplete and detailed results are lacking.

A paper by Jenny and Wyssmann [17] suggests the aerodynamic excitation is approximately two orders of magnitude smaller than other destabilizing mechanisms. Their simplified analysis, however, considers only the variation in radial clearance, while neglecting the change in momentum of the fluid. In a radial flow machine, the change in force due to clearance variations should be negligible compared to changes in force due to momentum variations since the former are perpendicular to the main flow path.

A paper by Washel and von Nimitz [18] gives an empirical formula for aerodynamic cross coupling forces in compressor impellers. It is used for comparison to the theory developed in this work.

The purpose of this paper [19] is to consider the nature and magnitude of aerodynamic cross-coupling forces and stiffnesses as generated by the change in fluid momentum in an eccentric impeller. The approach is to perform a control volume analysis on a perturbed, infinite bladed impeller undergoing a steady orbit at the rotational speed of the shaft. This assumes incompressible, ideal flow without volute or diffuser effects. It further assumes that the impeller consists of an infinite number of infinitely thin blades of simple geometry; the use of which allows an analytic expression for the aerodynamic forces to be obtained. Boundary layer development separation, and secondary flows, however, are not considered. The forces calculated are generated by a perturbation of the impeller about the flow center and thus are related to principal and cross-coupled stiffness terms. A separate analysis using a perturbation velocity would have to be performed in order to determine principal damping terms for the impeller.

2. VELOCITIES IN AN ECCENTRIC IMPELLER

Figure 1 shows a perturbed centrifugal impeller where 0′ is the geometric center of the impeller and 0 is the center of the steady flow field. It is assumed that the flow enters through an inlet pipe centered at 0 and the radial velocity varies inversely with radius away from this point. The eccentricity a is small such that the dimensionless eccentricity

$$\varepsilon = \frac{a}{R_1}$$

is much less than unity. For this analysis terms of order ε^2 and higher will be neglected. The impeller consists of an infinite number of infinitely thin logarithmic spiral blades with angle β. The blades are backward curved with a blade angle θ_b, an inner radius R_1, and outer radius R_2.

The analysis is to be performed in a coordinate system rotating at rotor speed ω about the center of the impeller. Only synchronous whirling about the flow center 0 will be considered. The fluid is assumed to follow the shape of the blades through the impeller passage and to exit parallel to the blades. The particle path in the absolute reference frame is shown in Figure 2. The impeller is purely two-dimensional and ideal, incompressible flow is assumed.

The radial inflow to a centered impeller in the fixed (non-rotating) coordinate system centered at 0 is

$$u = U_{R1} \frac{R_1}{r} \tag{1}$$

where the average inlet velocity is

$$U_{R1} = \frac{1}{2\pi} \int_0^{2\pi} u(R_1, \theta_1) d\theta_1$$

Here θ_1 is the angle of a fluid particle measured along $r = R_1$. The impeller rotates with angular velocity ω. The blade angle is given by

$$\tan \beta = \frac{U_{R1}}{\omega_{R1}}$$

From Fig. 1, the length R_B is

$$R_B = R_1 + a \cos\theta_1$$

Thus, along an eccentric impeller centered at 0′ the inlet velocity is

$$u = \frac{U_{R1} R_1}{(R_1 + a \cos\theta_1)} = U_{R1} \frac{1}{1 + \varepsilon \cos\theta_1} \tag{2}$$

From the binomial approximation

$$\frac{1}{1+\varepsilon\cos\theta_1} \simeq 1 - \varepsilon\cos\theta_1$$

which leads to

$$u = U_B = U_{R1}\ (1 - \varepsilon\cos\theta_1) \tag{3}$$

This is the assumed form of the flow entering the eccentric impeller at a point B around the impeller.

From the geometry of the eccentric impeller, this velocity can be resolved into components normal to and tangential to the impeller (shown in Fig. 3)

$$U_{BN} = U_B\cos\delta \simeq U_{R1}(1 - \varepsilon\cos\theta_1)$$

$$U_{BT} = -U_B\sin\delta \simeq -U_{R1}\ (1 - \varepsilon\cos\theta_1)\,\varepsilon\sin\theta_1 = -U_{R1}\ \varepsilon\sin\theta_1$$

for $\delta << 1$. The relative velocity of the rotating impeller is

$$V_B = \omega R_B = \omega R_1(1 + \varepsilon\cos\theta_1)$$

along the inner radius of the impeller. Resolving this velocity into normal and tangential components gives

$$V_{BN} = V_B\sin\delta \simeq \omega R_1\ \varepsilon\sin\theta_1 = \omega\ a\sin\theta_1$$

$$V_{BT} = V_B\cos\delta \simeq \omega R_1\ (1 + \varepsilon\cos\theta_1)$$

In the rotating coordinate system, the velocity of point B is $W_B = U_B - V_B$ or in components

$$W_{BN} = U_{R1}(1 - \varepsilon\cos\theta_1 - \varepsilon\cot\beta\sin\theta_1) \tag{4}$$

$$W_{BT} = -\omega_{R1}\ (1 + \varepsilon\cos\theta_1 + \varepsilon\tan\beta\sin\theta_1) \tag{5}$$

Since the tangential velocity does not enter the control volume, it will be neglected in this analysis.

From continuity, the radial velocity must vary inversely with r in the interior of the impeller. Let θ' denote the angle of the fluid particle as it travels along the log spiral blade relative to the x axis in the rotating coordinate system. The relative velocity of the fluid is then

$$W_N = U_{R1}\ \frac{R_1}{r}\ (1 - \varepsilon\cos\theta' - \varepsilon\cot\beta\sin\theta') \tag{6}$$

Let θ_2 denote the angle of the fluid particle at the exit of the impeller. Figure 2 shows that, in the rotating coordinate system, the fluid which enters the impeller at angle θ_1 also leaves the impeller at angle $\theta_1 - \theta_b$. Thus

$$\theta_2 = \theta_1 - \theta_b$$

The relative velocity at the exit of the impeller is, at $\theta' = \theta_2$,

$$W_{N2} = U_{R1} \frac{R_1}{R_2} (1 - \ddot{\varepsilon} \cos\theta_2 - \varepsilon \cot \beta \sin\theta_2)$$

For flow along a blade, the relative magnitude is given by

$$W_{TOT} = \left[W_N^2 + W_T^2 \right]^{1/2}$$

It is assumed that the number of blades is infinite so the streamlines follow the log spiral blade exactly.

$$\tan \beta = - \frac{W_T}{W_N} =$$

Then the magnitude becomes

$$W_{TOT} = \left[1 + (\tan \beta)^2 \right]^{1/2} W_N \tag{7}$$

where W_N is obtained from Eq. (6). While an exact representation of the variation of θ' with radius would be logarithmic, the approximation of a linear variation will be used to facilitate the development of an analytic expression. It is

$$\theta' = \theta - \frac{r - R_1}{R_2 - R_1} \theta_b$$

The total relative velocity vector has the angle β taken from the tangent to a circle of radius r. Thus the x and y components of $\vec{W}_{TOT}$ are given by

$$\vec{W}_{TOT} = W_{TOT} \left[\sin (\theta + \beta)\vec{i} - \cos (\theta + \beta)\vec{j} \right]$$

The general velocity expression becomes

$$\vec{W}_{TOT}(r,\theta) = U_{R1} \frac{R_1}{r} \left[1 + (\tan\beta)^2 \right]^{1/2} \left[1 - \varepsilon \cos \left(\theta - \frac{r - R_1}{R_2 - R_1} \right) - \varepsilon \cot \beta \sin \left(\theta - \frac{r - R_1}{R_2 - R_1} \right) \right] \left[\sin (\theta + \beta)\vec{i} - \cos (\theta + \beta)\vec{j} \right] \tag{8}$$

3. FORCE ON THE WHIRLING IMPELLER

The linear momentum equation for an accelerating control volume [20] is

$$\vec{F}_s - \int_{cv} [\vec{a} + 2\vec{\omega} \times \vec{V} + \vec{\omega}\times(\vec{\omega} \times \vec{r}) + \dot{\vec{\omega}} \times \vec{r}]\rho \, dv$$
$$= \frac{\partial}{\partial t} \int_{cv} \vec{V} \rho \, dv + \int_{cs} \vec{V} \rho(\vec{V} \cdot d\vec{A})$$

where

$\vec{F}_s$ = net surface forces acting on the control volume

$\vec{a}$ = rectilinear acceleration of the moving reference frame with respect to the fixed frame

$\vec{\omega}$ = angular velocity of the moving reference frame

$\vec{V}$ = velocity of a particle in the moving reference frame

$\dot{\vec{\omega}}$ = angular acceleration of the moving reference frame

$\vec{r}$ = position of a particle in the moving reference frame

For a reference frame rotating with constant angular velocity, this expression reduces to

$$\vec{F}_s = \int_{cv} [2\vec{\omega} \times \vec{V} + \vec{\omega} \times (\vec{\omega} \times \vec{r})] \rho dv + \int_{cs} \vec{V} \rho(\vec{V} \cdot d\vec{A}) \quad (9)$$

The surface forces consist of two parts

$$\vec{F}_s = \vec{F}_{SHAFT} + \vec{F}_p$$

where

$\vec{F}_{SHAFT}$ = force of shaft on control volume

$\vec{F}_p$ = pressure force acting on control volume

Bernoulli's equation for a rotating reference frame is

$$P - \frac{\rho}{2} |\vec{\omega} \times \vec{r}|^2 + \frac{\rho}{2} |\vec{V}|^2 = \text{CONST}$$

The pressure force on the control volume is given by

$$\vec{F}_p = - \int_{cs} P \, d\vec{A}$$

or, from Bernoulli's equation

$$\vec{F}_p = -\int_{cs} \left[\frac{\rho}{2}|\vec{\omega} \times \vec{r}|^2 - \frac{\rho}{2} |\vec{V}|^2\right] dA$$

The final expression for the force exerted by the shaft (impeller) on the fluid in the control volume is

$$\vec{F}_{SHAFT} = \int_{cv}\left[\rho\, 2\, \vec{\omega} \times \vec{V} + \rho\vec{\omega} \times (\vec{\omega} \times \vec{r})\right] dv$$

$$+ \int_{cs} \vec{V} \rho \vec{V} \cdot d\vec{A} + \int_{cs} \left[\frac{\rho}{2}|\vec{\omega} \times \vec{r}|^2 - \frac{\rho}{2} |\vec{V}|^2\right] dA$$

The desired force here is the force exerted by the fluid on the shaft. It is the negative of the above expression.

$$\vec{F}_{\substack{ON\\SHAFT}} = \underbrace{-\int_{cv} \rho\, 2\, \vec{\omega} \times \vec{V}\, dv}_{\text{Coriolis Force}} \underbrace{- \int_{cv} \rho\, \vec{\omega} \times (\vec{\omega} \times \vec{r})\, dv}_{\text{Centripital Force}}$$

$$\underbrace{-\int_{cs} \vec{V} \rho \vec{V} \cdot d\vec{A}}_{\substack{\text{Change in Linear}\\\text{Momentum}}} \underbrace{- \int_{cs} \frac{\rho}{2} |\vec{\omega} \times \vec{r}|^2\, dA}_{\substack{\text{Change in Pressure}\\\text{Due to Rotation}}} \qquad (10)$$

$$\underbrace{+ \int_{cs} \frac{\rho}{2} |\vec{V}|^2\, dA}_{\substack{\text{Change in Pressure Due}\\\text{to Change in Linear}\\\text{Momentum}}}$$

where

$$\vec{r} = (r + a \cos\theta)(\cos\theta\, \vec{i} + \sin\theta\, \vec{j})$$

$$\vec{\omega} = \omega\vec{k}$$

$$\vec{V} = \vec{W}_{TOT} = U_{R1} \frac{R_1}{r} \left[1 + (\tan\beta)^2\right]^{1/2} \left[1 - \varepsilon \cos\theta' - \varepsilon\cot\beta \sin\theta'\right]\left[\sin(\theta + \beta)\vec{i} - \cos(\theta + \beta)\vec{j}\right]$$

$$d\vec{A} = (\cos\theta\, \vec{i} + \sin\theta\, \vec{j})\, r\, d\theta\, dz$$

$$(\vec{V} \cdot d\vec{A}) = W_N - U_{R_1} \frac{R1}{r} (1 - \varepsilon \cos\theta' - \varepsilon \cot\beta \sin\theta')$$

$$dv = r\, d\theta\, dr\, dz$$

Integration is taken over the control volume from R_1 to R_2, and from 0 to 2π. On the control surface, integration is performed both at $r = R_2$ and at $r = R_1$ over θ from 0 to 2π. The thickness of the impeller is assumed to be the constant b.

For convenience in evaluation, the force acting on the shaft (impeller) due to the fluid is evaluated as five parts.

$$\vec{F}_{\substack{ON\\SHAFT}} = -\,①_{cv} - ②_{cv} - ③_{cs} - ④_{cs} + ⑤_{cs} \tag{11}$$

After integration, they are

Coriolis Force

$$① = 2\pi\, a\omega^2\rho\, b\, R_1 \left[\frac{R_2 - R_1}{\theta_b}\right] \tan\beta \left[1 + (\tan\beta)^2\right]^{1/2}$$

$$\times \Big\{ [-\sin(\theta_b + \beta) + \sin\beta - \cot\beta\cos(\theta_b + \beta) + \cot\beta\cos\beta]\vec{i}$$

$$+ [\cos(\theta_b + \beta) - \cos\beta - \cot\beta\sin(\theta_b + \beta) + \cot\beta\sin\beta]\vec{j} \Big\}$$

Centripetal Force

$$② = -\frac{1}{2}\pi\, a\, \omega^2\rho b\, (R_2^2 - R_1^2)\vec{i}$$

Change in Linear Momentum

$$③ = 2\pi\, a\omega^2\rho b\, R_1^2 \sin\beta\, (\tan\beta)^2\, [1 + (\tan\beta)^2]$$

$$\times \Big\{ -\Big[\frac{R_1}{R_2}\sin(\theta_b + \beta) - \frac{R_1}{R_2}\cot\beta\cos(\theta_b + \beta) + \sin\beta$$

$$+ \cot\beta\cos\beta\Big]\vec{i} + \Big[\frac{R_1}{R_2}\cos(\theta_b + \beta) - \frac{R_1}{R_2}\cot\beta\sin(\theta_b + \beta)$$

$$- \cos\beta + \cot\beta\sin\beta\Big]\vec{j} \Big\}$$

Change in Pressure Due to Rotation

(4) $= \pi a\omega^2 \rho b(R_2{}^2 - R_1{}^2)\vec{i}$

Change in Pressure Due to Change in Linear Momentum

(5) $$= \pi a\omega^2 \rho b\ R_1{}^2 (\tan\beta)^2\ [1 + (\tan\beta)^2]$$

$$\times \left\{ \left[- \frac{R_1}{R_2} \cos\theta_b + \frac{R_1}{R_2} \cot\beta \sin\theta_b + 1 \right] \vec{i} + \left[- \frac{R_1}{R_2} \sin\theta_b - \frac{R_1}{R_2} \cot\beta \cos\theta_b + \cot\beta \right] \vec{j} \right\}$$

The physical significance is indicated above each term.

The five parts can be summed together yielding the vector force acting on the shaft. Dividing the force into components gives F_{xx} and F_{yx}. A similar impeller eccentricity along the y axis would yield the forces F_{xy} and F_{yy}. What is of interest here is the stiffness obtained from

$$K_{ij} = - \frac{\Delta F_{ij}}{a}$$

The principal stiffness is

$$K_{xx} = - \pi\omega^2 \rho b\ R_1{}^2\ \left(\boxed{1} + \boxed{2} + \boxed{3} + \boxed{4} + \boxed{5} \right) \tag{12}$$

where

$$\boxed{1} = -2\ \frac{1}{\theta_b} (\bar{R} - 1)\ \tan\beta\ [1 + (\tan\beta)^2]^{1/2}$$

$$\times\ [-\sin(\theta_b + \beta) + \sin\beta + \cot\beta \cos(\theta_b + \beta) + \cot\beta \cos\beta]$$

$$\boxed{2} = \frac{1}{2} (\bar{R}^2 - 1)$$

$$\boxed{3} = -\ 2 \sin\beta\ (\tan\beta)^2\ [1 + (\tan\beta)^2]$$

$$\times \left[- \frac{1}{\bar{R}} \sin(\theta_b + \beta) - \frac{1}{\bar{R}} \cot\beta \cos(\theta_b + \beta) + \sin\beta + \cot\beta \cos\beta \right]$$

$$\boxed{4} = -\ (\bar{R}^2 - 1)$$

$$\boxed{5} = (\tan\beta)^2 [1 + (\tan\beta)^2]$$

$$\times \left[-\frac{1}{\bar{R}} \cos\theta_b + \frac{1}{\bar{R}} \cot\beta \sin\theta_b + 1 \right]$$

The cross-coupled stiffness is

$$K_{yx} = -\pi\omega^2\rho b\, R_1^2 \left(\triangle_1 + \triangle_3 + \triangle_5 \right) \tag{13}$$

where

$$\triangle_1 = -2\,\frac{1}{\theta_b}\,(\bar{R} - 1)\tan\beta\,[1 + (\tan\beta)^2]^{1/2}$$

$$\times\,[\cos(\theta_b + \beta) - \cot\beta\sin(\theta_b + \beta)]$$

$$\triangle_3 = -2\sin\beta\,(\tan\beta)^2\,[1 + (\tan\beta)^2]$$

$$\times\,[\frac{1}{\bar{R}}\cos(\theta_b + \beta) - \frac{1}{\bar{R}}\cot\beta\sin(\theta_b + \beta)]$$

$$\triangle_5 = (\tan\beta)^2\,[1 + (\tan\beta)^2]$$

$$\times\,[-\frac{1}{\bar{R}}\sin\theta_b - \frac{1}{\bar{R}}\cot\beta\cos\theta_b + \cot\beta]$$

Note that both principal and cross-coupled stiffnesses are obtained. In a rotor dynamics analysis, the other stiffnesses would be given by

$$K_{yy} = K_{xx}$$

$$K_{xy} = -K_{yx}$$

For comparison with other works and convenience in plotting results, the stiffnesses have been made dimensionless in the following manner

$$\bar{K}_{ij} = \frac{K_{ij}}{\rho U_{R_1}^{\;2} R_1} = \frac{K_{ij}}{\rho\omega^2 R_1^{\;3}\tan^2\beta}$$

The resulting expressions are

$$\bar{K}_{xx} = -\pi\,\frac{b}{R_1}\,\frac{1}{\tan^2\beta}\,(\triangle_1 + \triangle_2 + \triangle_3 + \triangle_4 + \triangle_5)$$

$$\bar{K}_{yx} = -\pi\,\frac{b}{R_1}\,\frac{1}{\tan^2\beta}\,(\triangle_1 + \triangle_3 + \triangle_5)$$

The dimenionless stiffnesses are functions of the ratio b/R_1, the radius ratio $\bar{R}$, the blade angle β, and angular sweep of the blade θ_b. The terms $\bar{R}$, β, and θ_b are related to one another so actually only two are independent. Also the term b/R_1 appears only as a multiplicative constant. Thus only the radius ratio $\bar{R}$ and the blade angle β need be varied for these stiffnesses.

4. RESULTS

Figure 4 shows a plot of the dimensionless stiffnesses $\bar{K}_{xx}$ and $\bar{K}_{yx}$ vs. blade angle β for a radius ratio $\bar{R} = 1.5$. For plotting purposes b/R_1 has been set to unity. It shows that the blade angle has a strong influence on both the magnitude and sign of the stiffnesses. The principal stiffness is large and positive for low blade angles. Pumps generally have a low blade angle so they fit in this category. The cross-coupled stiffness is negative for this level of blade angle. The large positive principal stiffness is generally a stabilizing effect while the negative $\bar{K}_{yx}$ term is destabilizing. In the range of pump blade angles, 10 to 20 degrees, the principal stiffness term is larger than the cross-coupled stiffness probably leading to an overall stabilizing effect. Compressors generally have large blade angles (as defined in this paper), perhaps in the range of 60 to 80 degrees. With a radius ratio $\bar{R} = 1.5$, both the principal stiffness and cross-coupled stiffness are negative indicating destabilizing effects. Field results indicate that pumps are usually stable while compressors are sometimes unstable. Thus the theory developed here appears to agree, at least qualitatively, with results from actual machines.

A semi-empirical formulation for the cross-coupled stiffness was developed in [18] of the form

$$K_{yx} = - \frac{6300\ HP\ (\mathrm{Mol\ Wt})\rho_o}{NDh\rho_s}$$

where

HP = pump horsepower

Mol Wt = fluid molecular weight

ρ_o = discharge density

ρ_s = suction density

N = speed in RPM

D = impeller diameter

h = restrictive dimension in flowpath

While this expression was developed for compressible flow, it can be reduced to incompressible flow. Non-dimensionalizing this reduced expression gives

$$\bar{K}_{yx} = -0.6\pi\ (b/R_1)\ n \cot\beta\ \bar{R}(\bar{R}-1)$$

where

n = the number of blades

$$HP = (\omega R_2)^2 - \omega U_{R_1} R_1 \cot\beta$$

The curve for this expression was added to Figure 4 with a blade number of eight. Another choice of number of blades will move the curve up or down somewhat without changing the overall shape of the curve. The plot of $\bar{K}_{yx}$ from the theory developed in this paper agrees fairly well with the semi-empirical formula.

Figure 5 gives the results for a radius ratio $\bar{R} = 2.0$. Again the principal stiffness is large for small blade angles. At larger blade angles, it decays to zero but does not go negative as it did for $\bar{R} = 1.5$. The cross-coupled stiffness is negative and fairly large over the blade angle range of 15 to 75 degrees. The semi-empirical formula gives a somewhat larger negative coefficient than the theory.

One of the purposes of this study is to examine the effects of various terms on the stiffnesses. Table 1 gives the five terms involved in the principal stiffness vs. blade angle for $\bar{R} = 1.5$. At low blade angles, the dominant effect is the change in pressure due to rotation. This term arises in Bernoulli's equation due to the rotating coordinate system. At larger blade angles, the dominant terms become the linear momentum ones. Now the other term from Bernoulli's equation is the largest but it is nearly balanced by the change in linear momentum. Table 2 shows the three terms in the cross-coupled stiffness vs. blade angle for $\bar{R} = 1.5$. At low blade angles, the Coriolis force produces the cross-coupled stiffness effect. At higher blade angles, the linear momentum terms become dominant. Tables 3 and 4 give the numerical values for $\bar{R} = 2.0$.

It is sometimes difficult to obtain a physical feel for the results of an analysis when dimensionless parameters are used. In an effort to impart a better idea of the numerical values developed from the theory here, some sample impellers were chosen. The results are given in Table 5. Generally small pumps will have very small stiffnesses while large pumps such as boiler feed pumps can have fairly large stiffness acting on them. The stiffness value here $K_{xx} = 124{,}000$ lbf/in is the same order of magnitude expected from the seals in a pump. A small compressor. even at high speed, produces a relatively small cross-coupling stiffness. Large compressors have somewhat larger coefficients. Often such a compressor will have eight or ten stages with a fairly flexible shaft. The cumulative effect can produce an instability.

5. CONCLUSIONS

The theoretical solution for a simple impeller model shows the principal and cross-coupled stiffnesses to be of about the same order of magnitude. For blade angles (β) less than thirty degrees, common for water pumps. the flow seems to provide tabilization for the shaft, while for the larger blade angles, common for compressors, the impeller is generally destabilizing. Since the magnitude of K_{xx} and K_{yx} are nearly the same, it would be important to include both terms in any rotor dynamics analysis of the shaft, rather than incorporating just the cross-coupling terms.

Though this work does not fully resolve the nature of aerodynamic forces on centrifugal machines, it does offer more understanding of these forces. An important element of any future work, however, is the availability of experimental data for verification. As of the present, no such data exists, although efforts are being perused in this area.

6. REFERENCES

1. Shepherd, D. G., Principles of Turbomachinery, MacMillan Publishing Co., New York, 1956.

2. Acosta, A. J., "An Experimental and Theoretical Investigation of Two-Dimensional Centrifugal Pump Impellers," Transactions of the ASME, July, 1954, p. 749-763.

3. Balje, O. E., "A Flow Model for Centrifugal Compressor Rotors," Transactions of the ASME, Vol. 100, Jan., 1978, p. 148-158.

4. Howard, J. H. G. and Lennemann, E.,"Measured and Predicted Secondary Flows in a Centrifugal Impeller," Journal of Engineering for Power, Trans. ASME, Jan., 1971, p. 126-131.

5. Lennemann, E. and Howard, J. H. G., "Unsteady Flow Phenomena in Rotating Centrifugal Impeller Passages," Journal of Engineering for Power, Trans. ASME, Jan. 1970, p. 65-72.

6. Moore, J., "A Wake and an Eddy in a Rotating Radial Flow Passage," Journal of Engineering for Power, Trans. ASME, July 1973, p. 205-219.

7. Alford, J. S., "Protecting Turbomachinery from Self-Excited Rotor Whirl," Journal of Engineering for Power, Trans. ASME, Oct. 1965, p. 333-344.

8. Black, H. F., "Lateral Stability and Vibration of High Speed Centrifugal Pump Rotors," IUTAM Dynamics of Rotors Symposium, Lyngby, Denmark, Aug. 1974, p. 56-74.

9. Barrett, L. E. and Gunter, E. J., "Stabilization of Aerodynamically Exicted Turbomachinery with Hydrodynamic Journal Bearings and Supports," Proceedings of NASA/ARO Workshop on Rotordynamic Instability Problems in High Performance Turbomachinery, College Station, Texas, May 1980.

10. Lund, J. W., "Some Unstable Whirl Phenomena in Rotating Machinery," The Shock and Vibration Digest, Vol. 7, No. 6, June 1975, p. 5-12.

11. Gunter, E. J., Barrett, L. E., and Allaire, P. E., "Stabilization of Turbomachinery with Squeeze Film Dampers - Theory and Application," I. Mech. E., Proceedings of Conference on Vibrations in Rotating Machinery, Cambridge, England, C233/76, Sept. 1976.

12. Colding-Jorgensen, J., "Effect of Fluid Forces on Rotor Stability of Centrifugal Compressors and Pumps," Proceedings of NASA/ARO Workshop on Rotordynamic Instability Problems in High-Performance Turbomachinery, College Station, Texas, May 1980.

13. Shoji, H. and Ohashi, H., "Fluid Forces on Rotating Centrifugal Impeller with Whirling Motion," Proceedings of NASA/ARO Workshop on Rotordynamic Instability Problems in High-Performance Turbomachinery, College Station, Texas, May 1980.

14. Thompson, W. E., "Vibration Exciting Mechanisms Induced by Flow in Turbomachine Stages," Proceedings of NASA/ARO Workshop on Rotordynamic Instability Problems in High-Speed Turbomachinery, College Station, Texas, May 1980.

15. Thompson, W. E., "Fluid Dynamic Excitation of Centrifugal Compressor Rotor Vibrations," Journal of Fluids Engineering, Vol. 100, March 1978, p. 73-78.

16. Chamieh, D. and Acosta, A. J., "Dynamic Forces on a Whirling Centrifugal Rotor," Proc. 6th Conference on Fluid Machinery, Akademiai Kiado, Budapest, Hungary, 1979.

17. Jenny, R. and Wyssmann, H. R., "Lateral Vibration Reduction in High Pressure Centrifugal Compressors," Proceedings of the Ninth Turbomachinery Symposium, Texas A&M University, Dec. 1980, p. 45-56.

18. Wachel, J. C. and von Nimitz, W. W., "Assuring the Reliability of Offshore Gas and Compression Systems," Proceedings of the European Offshore Petroleum Conference Vol. 1, EUR205, October, 1981, pp. 559-568.

19. Branagan, L. A., "Aerodynamic Forces on an Unbound Centrifugal Impeller: Effects of Change in Fluid Momentum," M.S. Thesis, University of Virginia, January, 1982.

20. Fox, R. W. and McDonald, A. T., Introduction to Fluid Mechanics, John Wiley & Sons, New York, 1978, p. 166.

TABLE 1. - EFFECT OF VARIOUS TERMS ON PRINCIPAL STIFFNESS FOR $\bar{R}$ = 1.5

Blade Angle	Coriolis Force	Centripetal Force	Change In Linear Momentum	Change In Pressure Due To Rotation	Change In Pressure Due To Change In Linear Momentum	Principal Stiffness
B	$\boxed{1}$	$\boxed{2}$	$\boxed{3}$	$\boxed{4}$	$\boxed{5}$	$\bar{K}_{xx}$
10.00	-.75	.63	-.09	-1.25	.03	144.75
15.00	-.67	.63	-.15	-1.25	.08	59.67
20.00	-.57	.63	-.21	-1.25	.15	29.76
25.00	-.50	.63	-.30	-1.25	.26	16.74
30.00	-.45	.63	-.44	-1.25	.44	10.05
35.00	-.42	.63	-.65	-1.25	.73	6.15
40.00	-.40	.63	-.98	-1.25	1.20	3.62
45.00	-.40	.63	-1.55	-1.25	2.00	1.80
50.00	-.41	.63	-2.55	-1.25	3.44	.33
55.00	-.43	.63	-4.46	-1.25	6.20	-1.05
60.00	-.47	.63	-8.44	-1.25	12.00	-2.59
65.00	-.53	.63	-17.78	-1.25	25.75	-4.66
70.00	-.63	.63	-43.96	-1.25	64.53	-8.04
75.00	-.81	.63	-140.25	-1.25	207.92	-14.94
80.00	-1.18	.63	-714.71	-1.25	1066.62	-34.20

TABLE 2. - EFFECT OF VARIOUS TERMS ON CROSS-COUPLED STIFFNESS FOR $\bar{R}$ = 1.5

Blade Angle	Coriolis Force	Change In Linear Momentum	Change In Pressure Due To Change In Linear Momentum	Cross-Coupled Stiffness	Cross-Coupled Stiffness
β	△1	△3	△5	$\bar{K}_{xy}$	Wachel [18]
10.00	.33	.03	.06	-42.96	-64.14
15.00	.71	.10	.09	-39.32	-42.21
20.00	.91	.18	.12	-28.73	-31.07
25.00	1.07	.27	.15	-21.52	-24.25
30.00	1.23	.38	.18	-16.84	-19.59
35.00	1.41	.53	.19	-13.69	-16.15
40.00	1.64	.74	.19	-11.46	-13.48
45.00	1.95	1.05	.11	-9.78	-11.31
50.00	2.37	1.53	-.11	-8.40	-9.49
55.00	3.00	2.32	-.70	-7.10	-7.92
60.00	3.96	3.71	-2.31	-5.62	-6.53
65.00	5.57	6.45	-6.93	-3.47	-5.27
70.00	8.52	12.65	-22.29	.47	-4.12
75.00	14.90	30.06	-87.79	9.66	-3.03
80.00	33.13	101.59	-533.98	39.00	-1.99

TABLE 3. - EFFECT OF VARIOUS TERMS ON PRINCIPAL STIFFNESS FOR $\bar{R}$ = 2.0

Blade Angle	Coriolis Force	Centripetal Force	Change In Linear Momentum	Change In Pressure Due To Rotating	Change In Pressure Due To Change in Linear Momentum	Principal Stiffness
β	$\boxed{1}$	$\boxed{2}$	$\boxed{3}$	$\boxed{4}$	$\boxed{5}$	$\bar{K}_{xx}$
10.00	-.89	1.50	-.09	-3.00	.03	247.42
15.00	-1.53	1.50	-.22	-3.00	.08	138.95
20.00	-1.58	1.50	-.35	-3.00	.15	77.74
25.00	-1.50	1.50	-.51	-3.00	.26	46.85
30.00	-1.42	1.50	-.73	-3.00	.44	30.17
35.00	-1.36	1.50	-1.06	-3.00	.73	20.43
40.00	-1.33	1.50	-1.59	-3.00	1.20	14.35
45.00	-1.33	1.50	-2.46	-3.00	2.00	10.35
50.00	-1.37	1.50	-4.00	-3.00	3.44	7.60
55.00	-1.45	1.50	-6.92	-3.00	6.20	5.64
60.00	-1.58	1.50	-12.95	-3.00	12.00	4.22
65.00	-1.79	1.50	-27.08	-3.00	25.75	3.16
70.00	-2.15	1.50	-66.57	-3.00	64.53	2.37
75.00	-2.76	1.50	-211.50	-3.00	207.92	1.77
80.00	-4.05	1.50	-1074.58	-3.00	1066.62	1.32

TABLE 4. - EFFECT OF VARIOUS TERMS ON CROSS-COUPLED STIFFNESS FOR $\bar{R}$ = 2.0

Blade Angle	Coriolis Force	Change in Linear Momentum	Change In Pressure Due To Change In Linear Momentum	Cross-Coupled Stiffness	Cross-Coupled Stiffness
β	△1	△3	△5	$\bar{K}_{xy}$	Wachel [18]
10.00	-.37	-.02	.09	30.89	-171.04
15.00	.44	.04	.14	-26.93	-112.56
20.00	1.12	.14	.19	-34.58	-82.86
25.00	1.63	.26	.25	-31.07	-64.68
30.00	2.07	.41	.33	-26.49	-52.24
35.00	2.52	.61	.41	-22.65	-43.07
40.00	3.03	.88	.50	-19.69	-35.94
45.00	3.69	1.28	.59	-17.44	-30.16
50.00	4.57	1.89	.64	-15.71	-25.31
55.00	5.84	2.89	.56	-14.31	-21.12
60.00	7.79	4.68	.00	-13.05	-17.41
65.00	11.00	8.18	-2.20	-11.60	-14.06
70.00	16.92	16.11	-10.85	-9.23	-10.98
75.00	29.68	38.40	-51.91	-3.65	-8.08
80.00	66.16	130.04	-353.46	15.36	-5.32

TABLE 5. - NUMERICAL EXAMPLES FOR PUMP AND COMPRESSOR IMPELLERS

Impeller	$\frac{\rho}{slug/ft^3}$	$\frac{\omega}{rpm}$	$\frac{R_1}{in}$	$\frac{b}{in}$	$\frac{\beta}{degrees}$	$\frac{K_{xx}}{lbf/in}$	$\frac{K_{yx}}{lbf/in}$
Small Pump	1.94	600	3.0	0.5	15	16.5	-3
Large Pump	1.94	10,000	9.0	1.5	15	124,000	-24,000
Small Compressor	7.5×10^{-3}	30,000	3.0	0.5	60	205	-702
Large Compressor	7.5×10^{-3}	10,000	12.0	0.5	60	720	-2,200

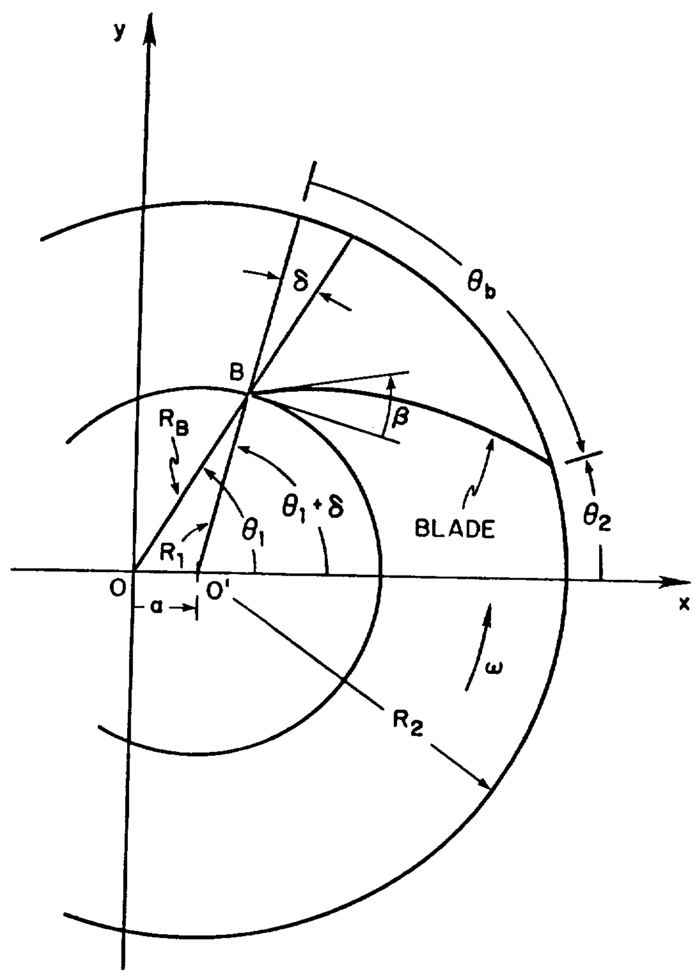

Figure 1. - Geometry of perturbed impeller.

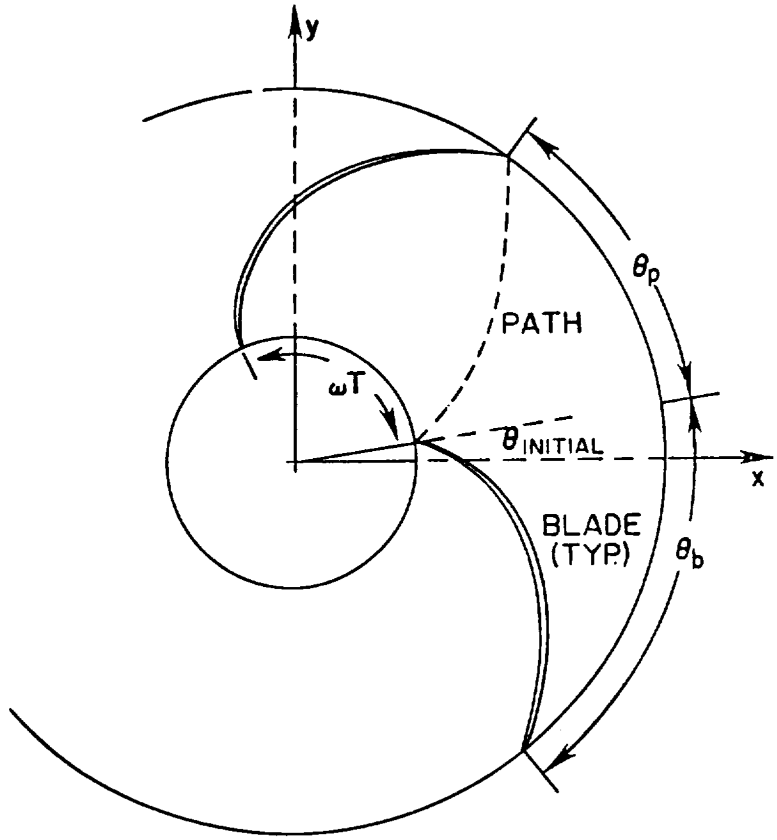

Figure 2. - Fluid path through impeller over passage time (T). Fixed coordinate frame [$\theta_p = \omega T - \theta_b$].

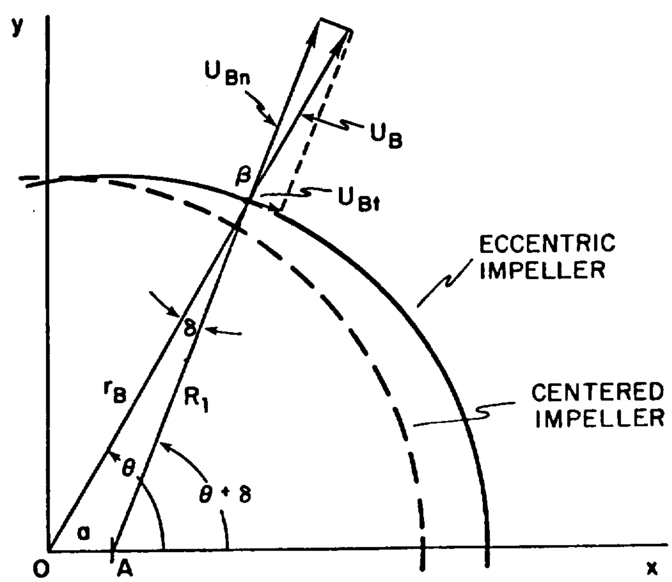

(a). Absolute velocity components at point B.

Figure 3. - Velocity components at impeller inlet.

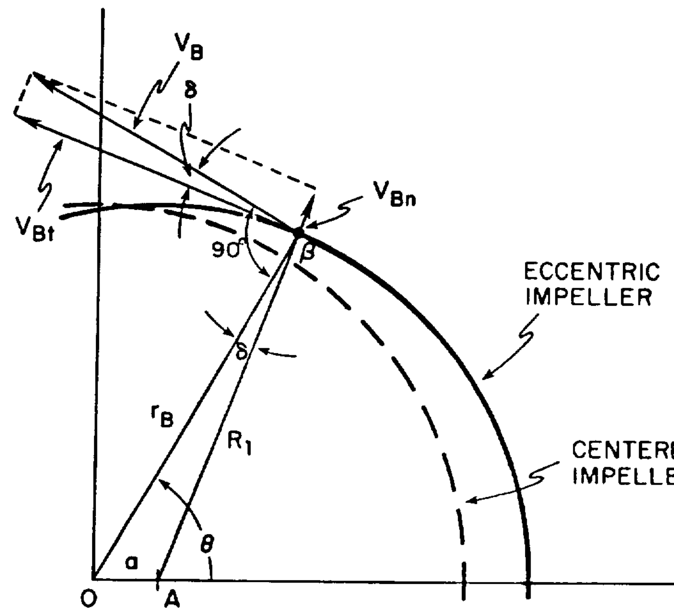

(b). Relative velocity between fluid and impeller.

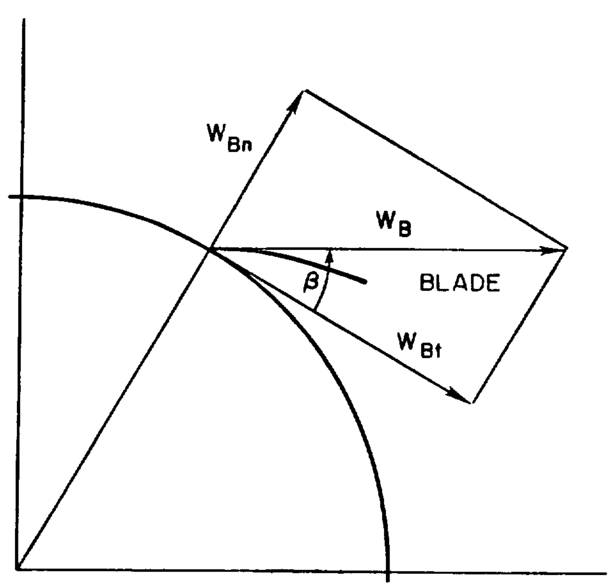

(c). Relative velocity components in rotating coordinate system.

Figure 3. - Concluded.

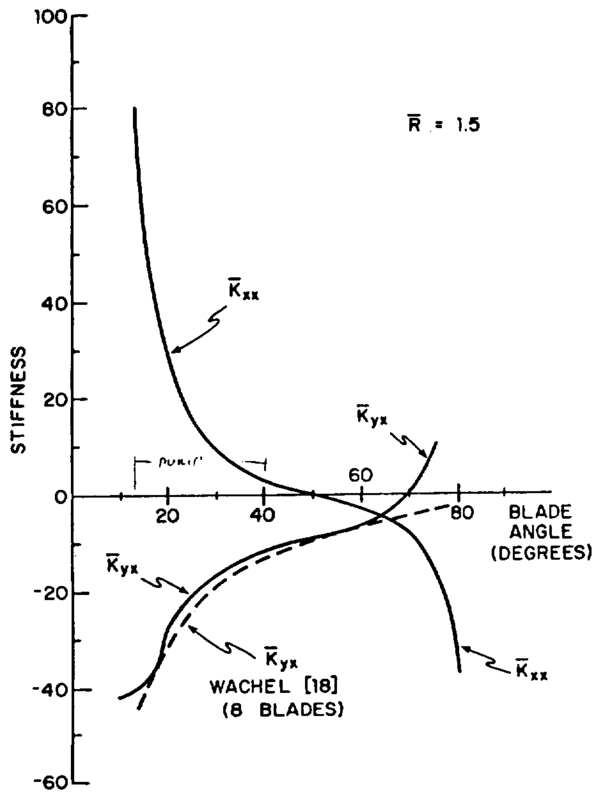

Figure 4. - Dimensionless stiffness versus blade angle for $\overline{R}$ = 1.5.

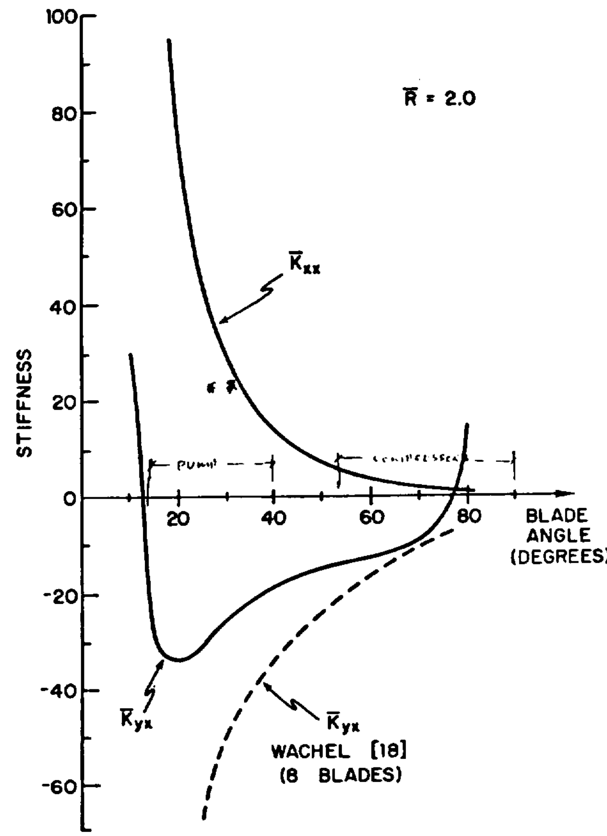

Figure 5. - Dimensionless stiffness versus blade angle for $\overline{R}$ = 2.0.